VIP Hydrogen Production Very Important Paper

Deutsche Ausgabe: DOI: 10.1002/ange.201603990
Internationale Ausgabe: DOI: 10.1002/anie.201603990

Boosting Photocatalytic Hydrogen Production of a Metal–Organic Framework Decorated with Platinum Nanoparticles: The Platinum Location Matters

Juan-Ding Xiao[+], Qichao Shang[+], Yujie Xiong, Qun Zhang, Yi Luo, Shu-Hong Yu, and Hai-Long Jiang**

Abstract: *Improving the efficiency of electron–hole separation and charge-carrier utilization plays a central role in photocatalysis. Herein, Pt nanoparticles of ca. 3 nm are incorporated inside or supported on a representative metal–organic framework (MOF), UiO-66-NH_2, denoted as Pt@UiO-66-NH_2 and Pt/UiO-66-NH_2, respectively, for photocatalytic hydrogen production via water splitting. Compared with the pristine MOF, both Pt-decorated MOF nanocomposites exhibit significantly improved yet distinctly different hydrogen-production activities, highlighting that the photocatalytic efficiency strongly correlates with the Pt location relative to the MOF. The Pt@UiO-66-NH_2 greatly shortens the electron-transport distance, which favors the electron–hole separation and thereby yields much higher efficiency than Pt/UiO-66-NH_2. The involved mechanism has been further unveiled by means of ultrafast transient absorption and photoluminescence spectroscopy.*

Hydrogen production from water splitting via photocatalysis, especially in the visible-light spectral region, has been the subject of intense research owing to its potential applications in clean and renewable energy. The development of highly efficient catalysts for maximizing the visible-light utilization and improving the efficiency of electron–hole separation remains critical in the field. To meet the challenges, various strategies and catalyst systems have been developed,[1] among which porous catalysts hold great promise because their porous structures allow for exposing active sites as much as possible and facilitate the accessibility of substrates to the active surface by reducing diffusion resistance. Particularly, as the photogenerated electrons undergo short transport distance to reach the substrates, the undesired volume recombination between electrons and holes can be largely avoided in the subsequent photocatalytic water reduction.[2]

As a type of porous materials, metal–organic frameworks (MOFs) have shown semiconductor-like characters in photocatalysis.[3–5] Some progress has been achieved by introducing visible-light-responsive units (e.g., organometallic complexes, 2-aminoterephthalate, porphyrin, etc.) into MOFs for visible-light photocatalytic hydrogen generation.[4] Notably, there have been several reports on photocatalysis over metal nanoparticles (NPs)/MOF composites, where metal NPs act as effective electron acceptors for spatial charge separation, leading to enhanced photocatalysis.[4d–f] However, to our knowledge, there has not been any targeted investigation on how the spatial position of electron acceptor influences the catalytic performance of MOF-based photocatalysts thus far. Given that most of the photoexcited electrons suffer from annihilation during their transport to the catalyst surface for reaction, it is recognized that the faster the electrons are trapped by the acceptor/cocatalyst, the higher the catalytic efficiency would be achieved. Thus, it would be highly desirable to gain fundamental understanding on the unexplored spatial-position effects of the electron acceptor in the MOF composite system.

The frequently used electron acceptors for enhanced photocatalysis are noble-metal NPs, especially Pt NPs,[4d–f,6] which can be immobilized in metal NPs/MOF composites by different strategies: in situ formation of metal NPs in MOFs,[7] and pre-synthesis of metal NPs for subsequent assembly of nanocomposites.[8] In this work, by adopting the pre-synthesis of metal NPs approach, Pt NPs of approximately 3 nm as electron acceptors are dispersed into or supported on a MOF, UiO-66-NH_2,[9] to afford Pt@UiO-66-NH_2 and Pt/UiO-66-NH_2, respectively (Scheme 1).

The UiO-66-NH_2 is chosen as it has an intersecting 3D structure, high stability, regular shape, and is visible-light responsive; meanwhile, the highly dispersed Pt NPs can be readily encapsulated/supported.[7a,b,8] Both Pt-decorated nanocomposites show an exponential enhancement of light-responsive activity in reference to the parent MOF. Remarkably, unlike the common core–shell structured photocatalysts with noble-metal NPs inside a semiconductor shell that disfavors the transportation of both charge and substrates, Pt NPs incorporated inside the semiconductor-like porous UiO-66-NH_2 are well accessible to protons. As a result,

[*] J.-D. Xiao,[+] Prof. Dr. Y. Xiong, Prof. Dr. S. H. Yu, Prof. Dr. H.-L. Jiang
Hefei National Laboratory for Physical Sciences at the Microscale, CAS Key Laboratory of Soft Matter Chemistry, Collaborative Innovation Center of Suzhou Nano Science and Technology, Department of Chemistry, University of Science and Technology of China
Hefei, Anhui 230026 (P.R. China)
E-mail: jianglab@ustc.edu.cn
Homepage: http://staff.ustc.edu.cn/~jianglab
Q. Shang,[+] Prof. Dr. Q. Zhang, Prof. Dr. Y. Luo
Synergetic Innovation Center of Quantum Information and Quantum Physics, Department of Chemical Physics, Hefei Science Center of CAS, University of Science and Technology of China
Hefei, Anhui 230026 (P.R. China)
E-mail: qunzh@ustc.edu.cn
[+] These authors contributed equally to this work.
Supporting information and the ORCID identification number(s) for the author(s) of this article can be found under http://dx.doi.org/10.1002/anie.201603990.

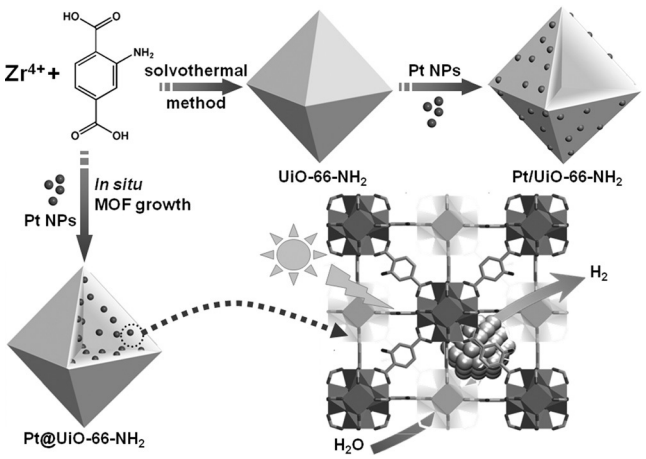

Scheme 1. Schematic illustration for the synthesis of Pt@UiO-66-NH_2 and Pt/UiO-66-NH_2, with the photocatalytic hydrogen production process over Pt@UiO-66-NH_2 being highlighted.

Pt@UiO-66-NH_2 greatly shortens the electron-transport distance and hence suppresses the electron–hole recombination, which is expected to have an enhanced catalytic activity compared to Pt/UiO-66-NH_2. In addition, the Pt NPs embedded in the MOF do not undergo aggregation or leaching during the reaction, which leads to better catalytic recyclability of Pt@UiO-66-NH_2 than that of Pt/UiO-66-NH_2. All these expectations and experimental results have been further verified by ultrafast transient absorption and photoluminescence spectroscopy characterizations.

The Pt NPs with uniform sizes of around 3 nm are synthesized following a published method (Figure S1 in the Supporting Information),[8] and then re-dispersed in DMF with $ZrCl_4$ and the ligand to afford Pt@UiO-66-NH_2 with different Pt loadings (Figure S2). The optimized Pt@UiO-66-NH_2 with 2.87 wt % Pt loading (determined by the inductively coupled plasma atomic emission spectrometry, ICP-AES) shows an excellent dispersion of Pt NPs inside the MOF particles (Figure 1 a,c). In parallel, the Pt/UiO-66-NH_2 with a similar Pt content (2.81 %) has been facilely prepared via

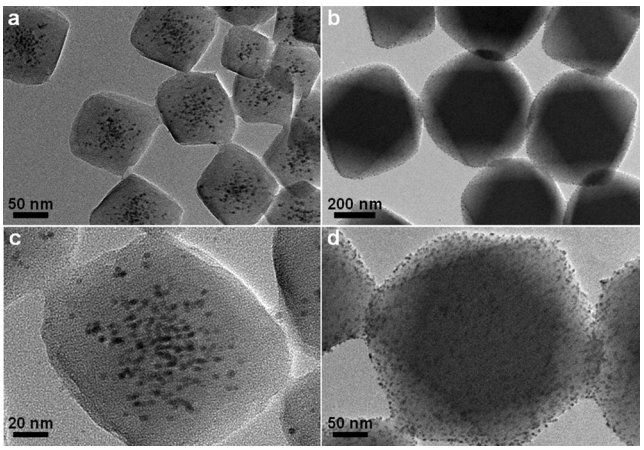

Figure 1. Typical TEM images of a),c) Pt@UiO-66-NH_2 and b),d) Pt/UiO-66-NH_2.

the assembly of Pt NPs in DMF solution with UiO-66-NH_2. The Pt/UiO-66-NH_2 features well-dispersed Pt NPs covering the whole external surface of the MOF particles (Figure 1 b,d). No aggregation occurs to Pt NPs and their sizes well maintain at around 3 nm in both samples based on transmission electron microscopy (TEM) observations (Figure 1, Figure S3). The crystallinity and structural integrity of UiO-66-NH_2 maintain well after Pt NPs are loaded, according to their similar powder X-ray diffraction (XRD) profiles and N_2 sorption at 77 K (Figure S4). All the above important features make it safe to conduct the following performance comparison between the Pt@UiO-66-NH_2 and Pt/UiO-66-NH_2 catalysts with a focus on their difference in the Pt location relative to MOF.

The UV/Vis diffuse reflectance spectra for Pt@UiO-66-NH_2 and Pt/UiO-66-NH_2 well inherit the feature of UiO-66-NH_2 and all the samples show roughly the same band gap (ca. 2.76 eV) and similar strong absorption in the region of approximately 300–450 nm, indicating their comparable light absorption (Figure 2 a). In addition, Pt@UiO-66-NH_2 has a more enhanced absorption than Pt/UiO-66-NH_2 and UiO-66-NH_2, which is most likely due to the close packing between Pt and UiO-66-NH_2 that leads to significantly high scattering at long wavelengths,[10] in agreement with the color change from pale yellow of UiO-66-NH_2 to dark gray of Pt@UiO-66-NH_2 (Figure S5). To unveil the charge-separation efficiency, photocurrent measurements have been carried out and the results show that the photocurrents for both Pt-decorated UiO-66-NH_2 get enhanced as compared to the pristine UiO-66-NH_2 (Figure 2 b), revealing that the formation of Pt-MOF Schottky junction helps to separate the photogenerated electron-hole pairs. The Pt@UiO-66-NH_2 displays much stronger photocurrent response than Pt/UiO-66-NH_2, suggesting the much higher efficiency of charge transfer from MOF to Pt NPs in the former. This argument is also supported by the electrochemical impedance spectroscopy (EIS) results (Figure 2 c), where Pt@UiO-66-NH_2 exhibits a smaller radius, indicative of a lower charge-transfer resistance. In addition, this is further verified by photoluminescence (PL) emission spectroscopy, which provides useful hints for the photoexcited charge transfer and recombination. The PL of UiO-66-NH_2 is slightly weakened when the Pt NPs are supported on the MOF, while get greatly suppressed when the Pt NPs are dispersed inside the MOF (Figure 2 d). These observations indicate that the radiative electron–hole recombination is more effectively suppressed by extracting the electrons with internal Pt than supported Pt. Such distinctly different photoelectrochemical properties in Pt@UiO-66-NH_2 and Pt/UiO-66-NH_2 unambiguously demonstrate that the Pt spatial location (inside or on the MOF particles) does matter.

Encouraged by the above characterization results, we set out to investigate the photocatalytic efficiency of Pt-MOF nanocomposites with different Pt locations. The water splitting for hydrogen production has been conducted with TEOA in CH_3CN as solvent under visible-light irradiation (Figure 3 a). As indicated in the previous reports,[4b,5b] for photocatalysis based on UiO-66-NH_2, the amino functionalized organic linker as an antenna can be excited by visible light to efficiently transfer energy to the Zr-oxo clusters via inter-

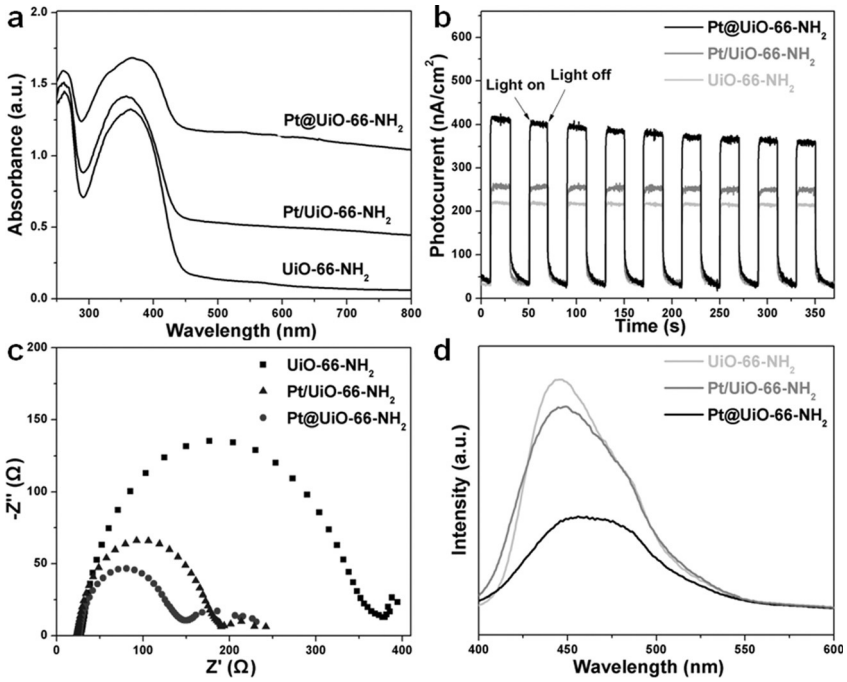

Figure 2. a) UV/Vis diffuse reflectance spectra, b) photocurrent responses, c) EIS Nyquist plots, and d) PL emission spectra (excited at 400 nm) for UiO-66-NH_2, Pt@UiO-66-NH_2, and Pt/UiO-66-NH_2.

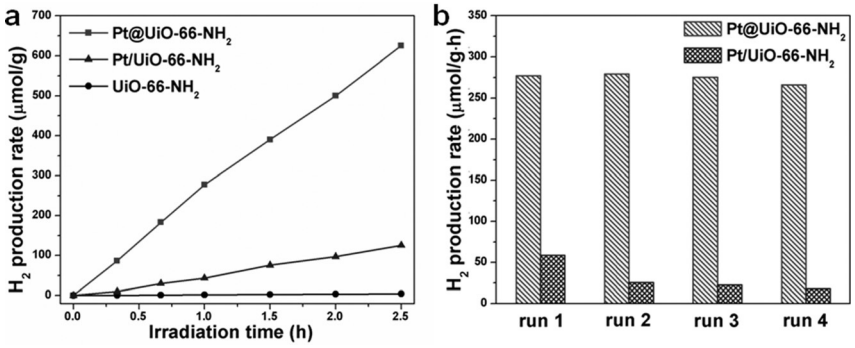

Figure 3. a) The photocatalytic hydrogen-production rates of UiO-66-NH_2, Pt@UiO-66-NH_2, and Pt/UiO-66-NH_2. b) Recycling performance comparison between Pt@UiO-66-NH_2 and Pt/UiO-66-NH_2.

system crossing. For Pt-decorated UiO-66-NH_2 catalysts, given that Pt with a low overpotential is an ideal electron trap and can provide redox reaction sites for hydrogen evolution, the photogenerated electrons on the MOF transfer to Pt through the Schottky junction for the subsequent proton reduction (Scheme S1). As displayed in Figure 3a, compared to the poor activity (1.72 $\mu mol\,g^{-1}\,h^{-1}$) of UiO-66-NH_2, the Pt/UiO-66-NH_2 exhibits around 30 times higher photocatalytic efficiency (50.26 $\mu mol\,g^{-1}\,h^{-1}$), revealing that the charge spatial separation between MOF and Pt plays a critical role in boosting its catalytic activity. Strikingly, the Pt@UiO-66-NH_2 exhibits a drastically enhanced activity (257.38 $\mu mol\,g^{-1}\,h^{-1}$), about 150 and 5 times higher than that of the parent MOF and Pt/UiO-66-NH_2, respectively, with similar Pt contents (2.87 vs. 2.81 wt%). Indeed, all Pt@UiO-66-NH_2 with different Pt loadings present much faster hydrogen-production rate than Pt/UiO-66-NH_2 (Figure S6), suggesting that photons are able to reach a high deepness through the outer MOF layer and almost all Pt NPs are assumed to be engaged in photocatalytic reaction (Supporting Information, Section 3). Further recycling experiments for Pt@UiO-66-NH_2 demonstrate that no noticeable change occurs in the hydrogen-production rate during the four catalytic runs for 10 h (Figure 3b). The powder XRD profiles confirm that the structural integrity and crystallinity of Pt@UiO-66-NH_2 are well retained after reaction (Figure S7). In contrast, the hydrogen-evolution rate over Pt/UiO-66-NH_2 reduces to one half after the first run and suffers from continued decrease in subsequent runs, which could be caused by undesired leaching or aggregation of Pt NPs. This assumption is further supported by the ICP (Table S1) and TEM results (Figure S8), the latter of which clearly show the aggregated Pt NPs on the MOF surfaces in the absence of strong protection, but well retained Pt dispersion in Pt@UiO-66-NH_2 due to the great confinement effect by the MOF structure.

The above photocatalysis results clearly demonstrate that, with all other parameters being fixed, the location of electron-injected Pt dominates the photocatalytic efficiency. Further, the electron spin resonance (ESR) results reveal the generation of Zr^{III} intermediate via electron transfer during photocatalysis over all the three samples (Figure S9).[5b,11] Interestingly, Pt@UiO-66-NH_2 gives the strongest Zr^{III} signal, which is most likely caused by the much accelerated electron-transfer process in Pt@UiO-66-NH_2, fitting well with the observed highest reaction rate.

To gain further insights into the involved electron-transfer processes, we resort to ultrafast transient absorption (TA) spectroscopy, a robust tool to track the real-time photoexcited carrier dynamics of nanocomposite systems.[5g,12] In the TA measurements, a scheme featuring femtosecond UV pump/white-light-continuum (WLC) probe is used. The pump laser is chosen at 400 nm (center wavelength), which can effectively promote electrons from the valence band to the conduction band of UiO-66-NH_2 (refer to the UV/Vis spectra in Figure 2a). The subsequent WLC probing in 540–750 nm, which manifests as positive absorbance changes, monitors the TA spectra of UiO-66-NH_2 at different probe delays (Figure 4a). It is found that different Pt location brings about no essential variation in the spectral profiles, but results in changes in the TA kinetics. Given that the relaxation kinetics of the TA

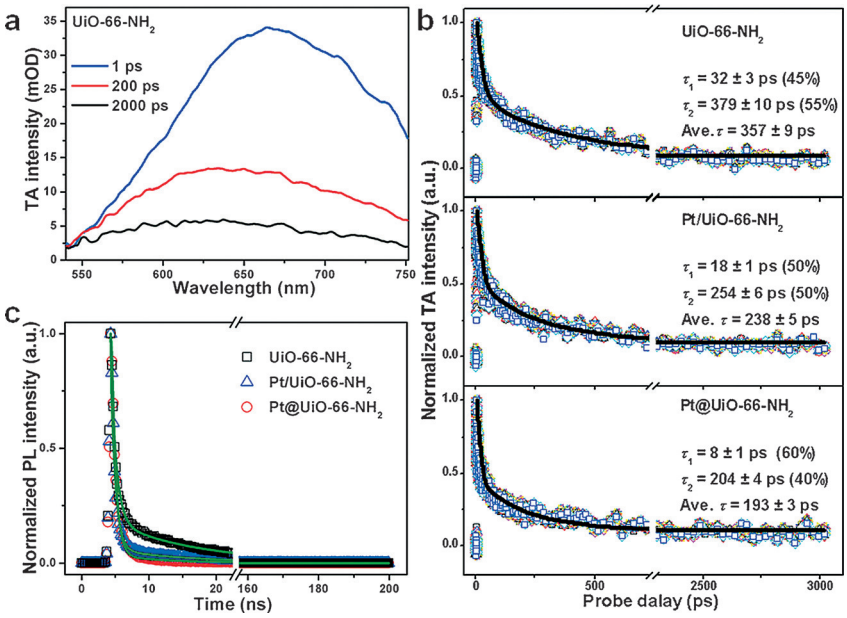

Figure 4. a) TA spectra of UiO-66-NH_2 (excitation at 400 nm) with TA signal given in mOD (OD: optical density). b) TA kinetics, and c) Time-resolved PL decay profiles for UiO-66-NH_2, Pt@UiO-66-NH_2, and Pt/UiO-66-NH_2, respectively (λ_{ex} = 400 nm, λ_{em} = 455 nm).

signal depends on the probing wavelength, we globally fit a set of kinetic traces ranging from 550 to 750 nm (21 traces with a 10-nm interval), as shown in Figure 4b. For each sample the TA signal builds up within the instrument response function (ca. 100 fs). The subsequent recovery is characterized by two time constants, that is, $\tau_1 = 32 \pm 3$ ps (45%) and $\tau_2 = 379 \pm 10$ ps (55%) for UiO-66-NH_2, $\tau_1 = 18 \pm 1$ ps (50%) and $\tau_2 = 254 \pm 6$ ps (50%) for Pt/UiO-66-NH_2, and $\tau_1 = 8 \pm 1$ ps (60%) and $\tau_2 = 204 \pm 4$ ps (40%) for Pt@UiO-66-NH_2. The mean relaxation lifetimes are 357 ± 9, 238 ± 5, and 139 ± 3 ps for UiO-66-NH_2, Pt/UiO-66-NH_2, and Pt@UiO-66-NH_2, respectively. Recovery featuring two decay components in the picosecond domain usually correlates to two trap states (probably with different trap depths),[13] namely, photogenerated electrons transfer from the conduction band minimum to a shallow trap state and then to a deep trap state. Since such trap states could be long-lived (normally in the nanosecond domain), time-resolved PL spectroscopy has been further examined. Figure 4c shows the PL kinetics for each sample at 455 nm emission (λ_{ex} = 400 nm). The mean PL lifetimes are determined to be 10.28 ± 0.06, 7.26 ± 0.04, 2.86 ± 0.02 ns for UiO-66-NH_2, Pt/UiO-66-NH_2, and Pt@UiO-66-NH_2, respectively.

On the basis of the combined results from the above TA and PL measurements, the pertinent mechanism underlying the photoexcited electron dynamics involved in the systems can be proposed. In comparison with UiO-66-NH_2, both Pt/UiO-66-NH_2 and Pt@UiO-66-NH_2 exhibit acceleration of TA decay kinetics, which should be attributed to the opening of an additional channel of electron transfer from the UiO-66-NH_2 to Pt NPs. The observations of PL quenching (Figure 2d) and shortening of the PL lifetime (Figure 4c) consistently suggest that the introduction of Pt NPs results in suppression of the photoexcited charge recombination in UiO-66-NH_2 due to the opening of such a new electron-transfer channel. More importantly, the comparison between Pt/UiO-66-NH_2 and Pt@UiO-66-NH_2 clearly indicates that a more efficient charge separation is achieved in the latter.

In conclusion, the uniform Pt NPs have been deliberately encapsulated inside or supported on MOF particles to afford Pt@UiO-66-NH_2 and Pt/UiO-66-NH_2, respectively, in which the only difference is the Pt location. Remarkably, the path of electron transfer from MOF to internal Pt is much shorter than to supported Pt, effectively avoiding the undesired volume charge recombination. Moreover, the electron-injected Pt NPs inside the MOF are readily available to protons, thanks to the high porosity of the MOF shell. As a result, Pt@UiO-66-NH_2 exhibits much better charge-carrier utilization and thus significantly higher photocatalytic hydrogen production activity than Pt/UiO-66-NH_2. In addition, the Pt@UiO-66-NH_2 catalyst possesses excellent stability and recyclability as a result of the great confinement for Pt NPs in the MOF, while Pt NPs in Pt/UiO-66-NH_2 are prone to leach and aggregate, resulting in the activity loss. Spectroscopic observations reveal the underlying electron-transfer mechanism and verify that a more efficient charge separation is achieved in the Pt@UiO-66-NH_2 case. The current study not only enables a deeper understanding on the electron-transfer mechanism for metal NPs-MOF composites, but also provides a unique perspective for the development of efficient MOF-based and even other porous material-based photocatalysts.

Acknowledgements

This work was supported by the NSFC (21371162, 21521001, 51301159, 21573211, 21421063), the 973 program (2014CB931803), the Strategic Priority Research Program of the Chinese Academy of Sciences (XDB01020000), the Recruitment Program of Global Youth Experts, and the Fundamental Research Funds for the Central Universities (WK2060190026, WK2340000063, WK2060190065).

Keywords: hydrogen production · metal–organic frameworks · photocatalysis · Pt nanoparticles · ultrafast spectroscopy

How to cite: *Angew. Chem. Int. Ed.* **2016**, *55*, 9389–9393
Angew. Chem. **2016**, *128*, 9535–9539

[1] a) Z. Zou, J. Ye, K. Sayama, H. Arakawa, *Nature* **2001**, *414*, 625; b) A. J. Esswein, D. G. Nocera, *Chem. Rev.* **2007**, *107*, 4022; c) A. Kudo, Y. Miseki, *Chem. Soc. Rev.* **2009**, *38*, 253; d) V. Artero, M. Chavarot-Kerlidou, M. Fontecave, *Angew. Chem. Int. Ed.* **2011**,

50, 7238; *Angew. Chem.* **2012**, *123*, 7376; e) Q. Xiang, J. Yu, M. Jaroniec, *J. Am. Chem. Soc.* **2012**, *134*, 6575; f) G. Xie, K. Zhang, B. Guo, Q. Liu, L. Fang, J. R. Gong, *Adv. Mater.* **2013**, *25*, 3820; g) T. Zhang, W. Lin, *Chem. Soc. Rev.* **2014**, *43*, 5982; h) D. Z. Zee, T. Chantarojsiri, J. R. Long, C. J. Chang, *Acc. Chem. Res.* **2015**, *48*, 2027.

[2] a) W. Zhou, W. Li, J.-Q. Wang, Y. Qu, Y. Yang, Y. Xie, K. Zhang, L. Wang, H. Fu, D. Zhao, *J. Am. Chem. Soc.* **2014**, *136*, 9280; b) Y. P. Xie, Z. B. Yu, G. Liu, X. L. Ma, H.-M. Cheng, *Energy Environ. Sci.* **2014**, *7*, 1895; c) B. Liu, L.-M. Liu, X.-F. Lang, H.-Y. Wang, X. W. Lou, E. S. Aydil, *Energy Environ. Sci.* **2014**, *7*, 2592; d) V. S. Vyas, F. Haase, L. Stegbauer, G. Savasci, F. Podjaski, C. Ochsenfeld, B. V. Lotsch, *Nat. Commun.* **2015**, *6*, 8508; e) Q. Lin, X. Bu, C. Mao, X. Zhao, K. Sasan, P. Feng, *J. Am. Chem. Soc.* **2015**, *137*, 6184.

[3] a) H.-C. Zhou, J. R. Long, O. M. Yaghi, *Chem. Rev.* **2012**, *112*, 673; b) H.-C. Zhou, S. Kitagawa, *Chem. Soc. Rev.* **2014**, *43*, 5415; c) J. Lee, O. K. Farha, J. Roberts, K. A. Scheidt, S. T. Nguyen, J. T. Hupp, *Chem. Soc. Rev.* **2009**, *38*, 1450; d) B. Chen, S. Xiang, G. Qian, *Acc. Chem. Res.* **2010**, *43*, 1115; e) G. Huang, Y.-Z. Chen, H.-L. Jiang, *Acta Chim. Sinica* **2016**, *74*, 113.

[4] a) Y. Kataoka, K. Sato, Y. Miyazaki, K. Masuda, H. Tanaka, S. Naito, W. Mori, *Energy Environ. Sci.* **2009**, *2*, 397; b) C. G. Silva, I. Luz, F. X. Llabrés i Xamena, A. Corma, H. García, *Chem. Eur. J.* **2010**, *16*, 11133; c) A. Fateeva, P. A. Chater, C. P. Ireland, A. A. Tahir, Y. Z. Khimyak, P. V. Wiper, J. R. Darwent, M. J. Rosseinsky, *Angew. Chem. Int. Ed.* **2012**, *51*, 7440 – 7444; *Angew. Chem.* **2012**, *124*, 7558 – 7562; d) C. Wang, K. E. deKrafft, W. Lin, *J. Am. Chem. Soc.* **2012**, *134*, 7211; e) Y. Horiuchi, T. Toyao, M. Saito, K. Mochizuki, M. Iwata, H. Higashimura, M. Anpo, M. Matsuoka, *J. Phys. Chem. C* **2012**, *116*, 20848; f) M. Wen, K. Mori, T. Kamegawa, H. Yamashita, *Chem. Commun.* **2014**, *50*, 11645; g) S. Pullen, H. Fei, A. Orthaber, S. M. Cohen, S. Ott, *J. Am. Chem. Soc.* **2013**, *135*, 16997; h) S. Saha, G. Das, J. Thote, R. Banerjee, *J. Am. Chem. Soc.* **2014**, *136*, 14845; i) T. Zhou, Y. Du, A. Borgna, J. Hong, Y. Wang, J. Han, W. Zhang, R. Xu, *Energy Environ. Sci.* **2013**, *6*, 3229.

[5] a) Y. Fu, D. Sun, Y. Chen, R. Huang, Z. Ding, X. Fu, Z. Li, *Angew. Chem. Int. Ed.* **2012**, *51*, 3364; *Angew. Chem.* **2012**, *124*, 3420; b) D. Sun, Y. Fu, W. Liu, L. Ye, D. Wang, L. Yang, X. Fu, Z. Li, *Chem. Eur. J.* **2013**, *19*, 14279; c) K. G. M. Laurier, F. Vermoortele, R. Ameloot, D. E. De Vos, J. Hofkens, M. B. J. Roeffaers, *J. Am. Chem. Soc.* **2013**, *135*, 14488; d) L. Li, S. Zhang, L. Xu, J. Wang, L.-X. Shi, Z.-N. Chen, M. Hong, J. Luo, *Chem. Sci.* **2014**, *5*, 3808; e) S. Wang, W. Yao, J. Lin, Z. Ding, X. Wang, *Angew. Chem. Int. Ed.* **2014**, *53*, 1034; *Angew. Chem.* **2014**, *126*, 1052; f) L. Shi, T. Wang, H. Zhang, K. Chang, J. Ye, *Adv. Funct. Mater.* **2015**, *25*, 5360; g) H.-Q. Xu, J. Hu, D. Wang, Z. Li, Q. Zhang, Y. Luo, S.-H. Yu, H.-L. Jiang, *J. Am. Chem. Soc.* **2015**, *137*, 13440.

[6] J. Yang, D. Wang, H. Han, C. Li, *Acc. Chem. Res.* **2013**, *46*, 1900.

[7] a) H. Liu, L. Chang, C. Bai, L. Chen, R. Luque, Y. Li, *Angew. Chem. Int. Ed.* **2016**, *55*, 5019; *Angew. Chem.* **2016**, *128*, 5103; b) Z. Guo, C. Xiao, R. V. Maligal-Ganesh, L. Zhou, T. W. Goh, X. Li, D. Tesfagaber, A. Thiel, W. Huang, *ACS Catal.* **2014**, *4*, 1340; c) P. Hu, J. V. Morabito, C.-K. Tsung, *ACS Catal.* **2014**, *4*, 4409; d) Y. Liu, Z. Tang, *Adv. Mater.* **2013**, *25*, 5819; e) A. Aijaz, A. Karkamkar, Y. Choi, N. Tsumori, E. Rönnebro, T. Autrey, H. Shioyama, Q. Xu, *J. Am. Chem. Soc.* **2012**, *134*, 13926; f) Q.-L. Zhu, Q. Xu, *Chem. Soc. Rev.* **2014**, *43*, 5468; g) L. Shen, M. Luo, L. Huang, P. Feng, L. Wu, *Inorg. Chem.* **2015**, *54*, 1191; h) Y.-Z. Chen, Y.-X. Zhou, H. Wang, J. Lu, T. Uchida, Q. Xu, S.-H. Yu, H.-L. Jiang, *ACS Catal.* **2015**, *5*, 2062.

[8] a) K. Na, K. M. Choi, O. M. Yaghi, G. A. Somorjai, *Nano Lett.* **2014**, *14*, 5979; b) W. Zhang, G. Lu, C. Cui, Y. Liu, S. Li, W. Yan, C. Xing, Y. Chi, Y. Yang, F. Huo, *Adv. Mater.* **2014**, *26*, 4056.

[9] M. Kandiah, M. H. Nilsen, S. Usseglio, S. Jakobsen, U. Olsbye, M. Tilset, C. Larabi, E. A. Quadrelli, F. Bonino, K. P. Lillerud, *Chem. Mater.* **2010**, *22*, 6632.

[10] S. Sarina, H.-Y. Zhu, Q. Xiao, E. Jaatinen, J. Jia, Y. Huang, Z. Zheng, H. Wu, *Angew. Chem. Int. Ed.* **2014**, *53*, 2935; *Angew. Chem.* **2014**, *126*, 2979.

[11] a) M. Occhiuzzi, D. Cordischi, R. Dragone, *J. Phys. Chem. B* **2002**, *106*, 12464; b) J. Long, S. Wang, Z. Ding, S. Wang, Y. Zhou, L. Huang, X. Wang, *Chem. Commun.* **2012**, *48*, 11656.

[12] a) R. Li, J. Hu, M. Deng, H. Wang, X. Wang, Y. Hu, H.-L. Jiang, J. Jiang, Q. Zhang, Y. Xie, Y. Xiong, *Adv. Mater.* **2014**, *26*, 4783; b) F. Lei, L. Zhang, Y. Sun, L. Liang, K. Liu, J. Xu, Q. Zhang, B. Pan, Y. Luo, Y. Xie, *Angew. Chem. Int. Ed.* **2015**, *54*, 9266; *Angew. Chem.* **2015**, *127*, 9398; c) K. Wu, H. Zhu, T. Lian, *Acc. Chem. Res.* **2015**, *48*, 851.

[13] D. A. Wheeler, J. Z. Zhang, *Adv. Mater.* **2013**, *25*, 2878.

Received: April 25, 2016
Published online: June 20, 2016

